Journal of Neuroinflammation

RESEARCH

Open Access

Complement inhibition targets a rich-club within the neuroinflammatory network after stroke to improve radiographic and functional outcomes

Youssef M. Zohdy[1], Tomas Garzon-Muvdi[1], Jonathan A. Grossberg[1], Daniel L. Barrow[1], Brian M. Howard[1], Gustavo Pradilla[1], Firas H. Kobeissy[2], Stephen Tomlinson[3,4] and Ali M. Alawieh[1*]

Abstract

Following recent advances in post-thrombectomy stroke care, the role of neuroinflammation and neuroprotective strategies in mitigating secondary injury has gained prominence. Yet, while neuroprotection and anti-inflammatory agents have re-emerged in clinical trials, their success has been limited. The neuroinflammatory response in cerebral ischemia is robust and multifactorial, complicating therapeutic approaches targeting single pathways. In this study, we aimed to characterize early inflammatory gene dysregulation following ischemic stroke using translational in-silico and in-vivo approaches. Using an in vivo ischemic stroke model, transcriptomic analysis revealed significant dysregulation of inflammatory genes. Graph theory analysis then showed a rich-club organization among stroke-related genes, with highly connected core nodes. The expression levels of the core genes identified within this network significantly explained radiological outcomes, including T2-signal hyperintensity ($R^2 = 0.57$, $P < 0.001$), mean diffusivity ($R^2 = 0.52$, $P < 0.001$), and mean kurtosis ($R^2 = 0.65$, $P < 0.001$), correlating more strongly than non-core genes. Similar findings were observed with functional and cognitive outcomes, showing R^2 values of 0.58, 0.7, 0.54, and 0.7 for neurological severity scores, corner tasks, passive avoidance, and novel object recognition tasks, respectively ($P < 0.001$). Using in-silico analysis, we identified a set of upstream regulators directly interacting with core network nodes, leading to simulations that highlighted C3-targeted therapy as a potential treatment. This hypothesis was then confirmed in vivo using a targeted C3 inhibitor (CR2-fH), which reversed gene dysregulation in the neuroinflammatory network and improved radiological and functional outcomes. Our findings underscore the significance of neuroinflammation in stroke pathology, supporting network-based therapeutic targeting and demonstrating the benefits of targeted complement inhibition in enhancing outcomes through modulation of the neuroinflammatory network core. This study's approach, combining graph theory analysis along with in-silico modeling, offers a promising translational pipeline applicable to stroke and other complex diseases.

Keywords Stroke, Rich-club, Network analysis, Transcriptomics, Complement inhibition

*Correspondence:
Ali M. Alawieh
ali.mostafa.alawieh@emory.edu
Full list of author information is available at the end of the article

Introduction

Following the revolution in stroke care in the post-thrombectomy area[1–5], the role of neuroinflammation and the significance of neuroprotective strategies in mitigating secondary injury have become increasingly apparent[6, 7]. Despite the substantial success of mechanical recanalization trials, only approximately 50% of patients who underwent successful procedures achieved functional independence at 90 days, emphasizing the need for adjuvant interventions [8–10]. After a period of diminished interest, clinical trials focusing on neuroprotection and anti-inflammatory agents have regained prominence in the context of reperfusion therapies, albeit with limited success to date [11–13].

The role of the neuroinflammatory response in cerebral ischemia is well-established, and work from our group and others has studied the triggers and sequelae of immune system activation in the ischemic brain [8, 14–18]. The post-ischemic neuroinflammatory response is robust and multifactorial, posing a major challenge for therapeutic strategies relying on single drug targets. Despite this complexity, numerous key regulators have been identified at various phases of the response and have been targeted in preclinical therapeutic strategies. Our previous work characterized the role of the complement system in the early recognition of injury after stroke, and demonstrated its involvement in the activation and amplification of downstream neuroinflammatory pathways. We have shown that site-targeted complement inhibitors can enhance stroke recovery in both reperfused and non-reperfused stroke models. However, the mechanistic effects of complement-dependent pathology remain under-investigated [6, 8, 9, 15, 18–23].

In this study, we aimed to characterize the early inflammatory gene dysregulation that occurs after ischemic stroke and apply graph theory concepts to identify core regulators within the network, focusing on their relationships to radiographic and functional outcomes as well as responses to therapeutic interventions. Using differentially expressed genes (DEGs) from an in vivo ischemic stroke model, we constructed a post-ischemic neuroinflammatory network. Network analysis revealed a rich-club organization among key regulators, and we assessed the selective impact of this rich-club on functional and radiographic outcomes. Furthermore, we investigated the effects of targeted complement inhibition on the identified core network genes and its subsequent impact on cognitive and functional outcomes using both in-silico and in-vivo models. This study also provides a novel pipeline of complementary in-silico and in-vivo analyses for therapeutic disease targeting.

Methods

Murine Stroke Model

We used the transient middle cerebral artery occlusion (MCAO) model in adult C57BL/6j mice (Jackson Laboratories) to mimic clinical stroke and mechanical reperfusion. The model has been described in detail previously by our group [8, 9, 19]. Mice were 12 weeks old at the time of surgery which followed a 2-week acclimation period. Only male mice were used in this study. Anesthesia was induced using intraperitoneal injection of ketamine (80 mg/kg) and xylazine (10 mg/kg). Anesthesia level was monitored using toe pinch, and vital signs were monitored during the procedure and recovery. Transient MCAO (tMCAO) was induced by advancing a rounded blunt-tip 5–0 nylon suture through the internal carotid artery to the origin of the MCA as previously described[8, 9, 19, 24]. Laser Doppler flow monitoring (moorVMS-LDF1 device; Moor Instruments) was employed to ensure consistent induction of ischemia, and animals with less than 80% reduction in ipsilateral cerebral blood flow compared to the presurgical baseline were excluded from the study. Following 60 min, the suture was removed to allow for reperfusion. There were no significant differences in weight, heart rate, respiratory rate, or degree of blood flow reduction among the various treatment groups ($p > 0.05$). Postoperatively, animals were housed in a chamber with controlled temperature and humidity until fully recovered from anesthesia and returned to their assigned housing. No significant differences in intra- and peri-procedural temperatures were observed between the different groups. Sham operations included the same surgical approach including skin incision and ligation of the external carotid artery but no intraluminal filament placement. Laser Doppler flow monitoring was used to confirm that there was no reduction in ipsilateral cerebral blood flow compared to the presurgical baseline. Perioperatively, no analgesics were administered to avoid anti-inflammatory effects; instead, supportive care and a soft gel diet were provided.

A total of twenty-eight animals were used in this study. Four mice underwent sham surgery, while twenty-four mice underwent tMCAO. Four mice were excluded from the tMCAO group: three did not meet the required cerebral blood flow criteria, and one had immediate postoperative mortality. The remaining mice were equally randomized into treatment groups. All animal procedures were approved by the Institutional Animal Care and Use Committee (IACUC) at the Medical University of South Carolina (MUSC). The overall experimental approach is summarized in Fig. 1.

Magnetic resonance imaging

MRI scans were conducted on day 4 post-stroke using a 7 T/30 Bruker Biospec animal scanner at the Center for Biomedical Imaging at MUSC. Anatomic T1 images and T2-weighted imaging were obtained. Lesion size, as a composite measure of infarct and associated edema, was estimated from T2-weighted imaging following 3D-reconstruction of volume from 15 2-mm-thick slices on ThermoFisher Amira 2023. We also obtained both diffusion tensor imaging (DTI) and diffusion kurtosis imaging (DKI) as previously described [8]. DTI images were captured using a 2-shot spin-echo echo planar diffusion sequence with 30 diffusion-encoding directions and 3 b values: 0, 1000, and 2000s/mm^2. Detailed imaging parameters included a repetition time of 3750 ms, echo time of 3750/32.5 ms, field of view of 30 mm × 30 mm, matrix size of 128 × 128, and number of excitations set to 2. A total of 15 axial slices with no interslice gap were acquired at a thickness of 2 mm. Diffusion and diffusional kurtosis tensors were computed using the diffusional kurtosis estimator[25]. Regions of interest (ROIs) were delineated over the basal ganglia in the ipsilateral (stroke) hemisphere. Corresponding ROIs were symmetrically drawn in the contralesional hemisphere, and the ratio of ipsilateral-to-contralateral mean diffusivity (MD) and mean kurtosis (MK) were determined. MD and MK represent the averaged apparent diffusion and kurtosis coefficients across all directions, respectively.

Sensorimotor recovery

Functional recovery was evaluated daily by two unbiased observers using the previously defined neurological severity score [8, 9, 26]. This scoring system assigned a score of 0 for normal motor function, 1 for torso and contralateral forelimb flexion upon tail elevation, 2 for contralateral circling when held by the tail on a flat surface, 3 for contralateral leaning at rest, and 4 for the absence of spontaneous motor activity. Daily assessment was performed, and to avoid bias due to mortality, a last observation carried forward approach was used. Forelimb asymmetry was assessed using the corner test as previously reported [27]. Briefly, a mouse is placed between two boards set at a 30° angle, with a small opening along the joint to encourage entry into the corner. The mouse is placed midway between the boards, facing the corner. As the mouse enters the corner, both sides of its vibrissae are stimulated simultaneously. The mouse then rears upward and forward before turning to face the open end. A non-ischemic mouse typically turns either left or right, while the ischemic mouse preferentially turns toward the non-impaired side. Turning directions were recorded across ten trials for each test, with turns not associated with rearing excluded from the count. Animals were acclimated to the test environment prior to induction of tMCAO over 2 days, and baseline forearm preference was documented. Animals were then tested post-operatively (day 4) and performance was compared to pre-operative baseline using the normalized laterality index [27].

Cognitive recovery

Two independent behavioral assessments were used for the measurement of cognitive recovery as relevant to the anatomic location of the MCA. We used the passive avoidance (PA) task and novel object recognition (NOR) tasks to assess cognitive recovery after MCAO. For PA, animals were trained to associate a shock with the dark chamber of a double chamber box and were subsequently tested at baseline and post-stroke to assess retention of avoidance memory, measured by the time taken to enter the dark chamber using an automated passive avoidance apparatus equipped with automated sensing and shock systems (Coulbourn Instruments; GraphicState 4) [8, 19]. NOR task was performed as previously described [28], and outcomes were assessed based on the percentage time spent next to familiar versus novel objects in

(See figure on next page.)

Fig. 1 Study design and analytical pipeline. **a** Adult C57BL/6 J mice were randomized into either a sham group or subjected to 60 min of transient middle cerebral artery occlusion (MCAO). **b**–**c** behavioral testing included neurological severity score (NSS) performed daily, corner task performed on day 4, novel object recognition task (NOR) performed on day 3, and passive avoidance (PA) performed on day 4. **(c)** MRI scans were conducted on day 4 post-stroke using a 7 T/30 Bruker Biospec animal scanner including T2-weighted imaging, diffusion tensor imaging (DTI) and diffusion kurtosis imaging (DKI). **d** Mice were sacrificed 5 days post-MCAO, and ipsilateral hemisphere representing the MCA territory was harvested, and homogenized for RNA extraction. **e** RNA was extracted using the RNeasy Lipid Tissue kit (Qiagen). **f** High-throughput analysis of immunology-related gene expression was carried out using the Nanostring Mouse Immunology Codeset comprising 561 genes. **g** Expression data were analyzed, and differentially expressed genes (DEGs) were identified. **h** Gene Ontology analysis was used to functionally annotate the DEGs. **i** Using gene interaction data from the STRING database and the weighted gene co-expression network analysis (WGCNA) algorithm, a gene interaction network was constructed using the identified DEGs. **j** Graph theory methodology was then used to identify the network hub genes, known as "rich-club" genes. **k** Ingenuity Pathway Analysis (IPA) software was used to identify upstream regulators of the rich-club genes, and the results were visualized using Cytoscape. **l** In vivo inhibition of C3 activation, an IPA-identified target, was conducted in a similar paradigm to (**a**), and the correlation between treatment and outcomes was analyzed

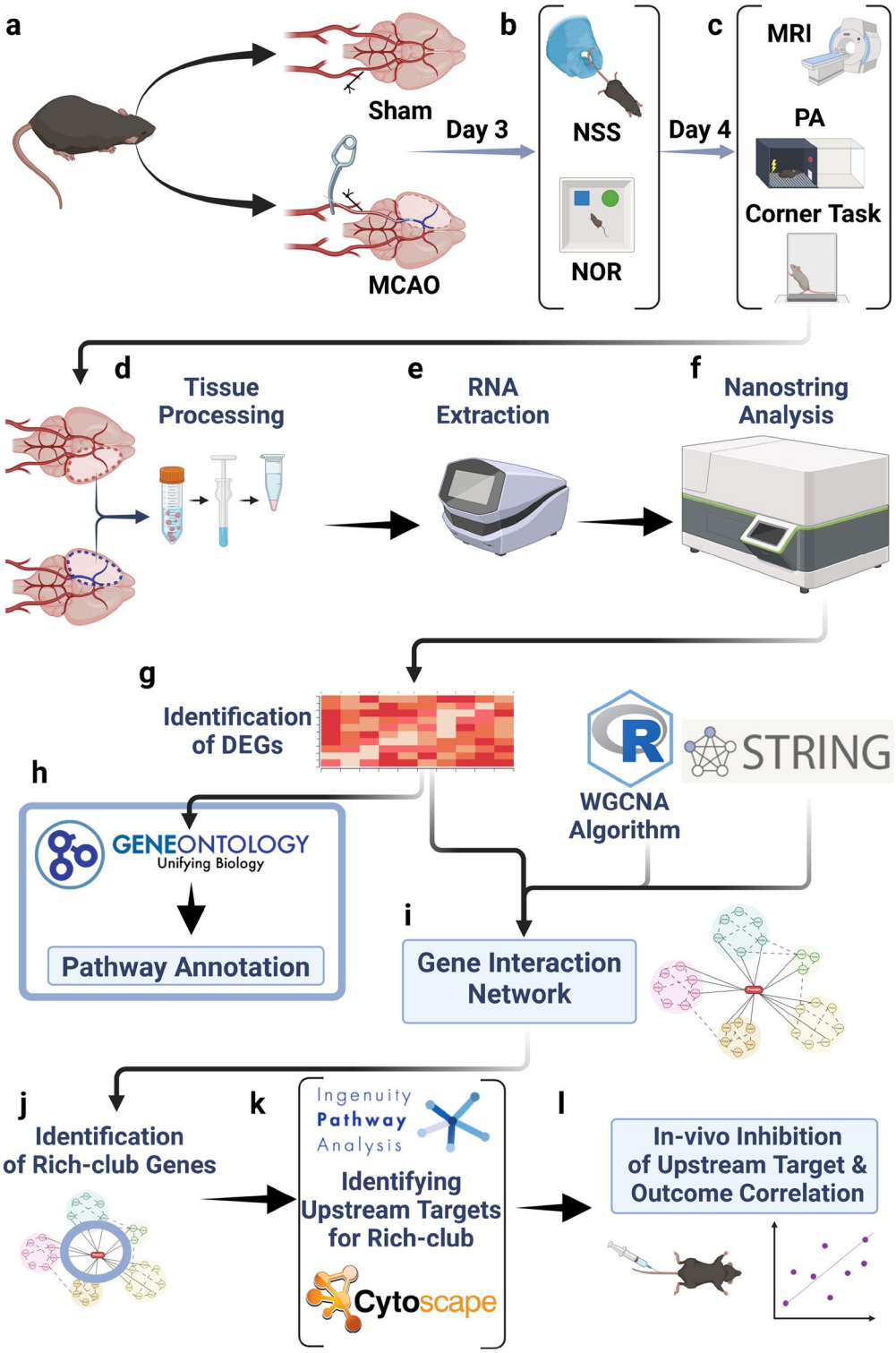

Fig. 1 (See legend on previous page.)

an open field platform after a period of acclimation [6, 8, 9, 19, 26, 28]. Open-field locomotor activity was used to establish the absence of baseline differences in anxiety levels between the different groups on the days of testing by comparing time spent at the center and periphery of the field prior to object placement.

Recombinant protein preparation and testing

To achieve site-targeted complement inhibition, we used a recombinant fusion protein of complement receptor 2 (CR2) and the inhibitor of the alternative complement pathway factor H which we have previously described[8, 16, 19]. Plasmids encoding the fusion protein, CR2-fH, were transfected into Chinese hamster ovary (CHO) cells and the recombinant protein was then purified from supernatant as previously described[29]. Purified proteins were tested for endotoxin and for complement inhibitory activity using both chicken red blood cell lysis assay and zymosan assay as described previously[19, 29]. CR2-fH has been shown to localize specifically to the ischemic penumbra and inhibit the amplification of C3 activation via the alternative complement pathway locally after murine stroke[8, 19].

Animal treatment

Following tMCAO, mice were randomized, using an automated in-house script, to receive either vehicle (phosphate-buffered saline, N = 10) or CR2-fH (16 mg/kg, N = 10) at 2 h after reperfusion via a tail vein injection. Animals were then returned to their cages and tested for recovery as described before. To ensure the integrity of the results, the operators performing the surgical procedures, administering injections, and evaluating outcomes were blinded to the group allocations.

Nanostring gene expression analysis

High-throughput analysis of immunology-related gene expression was carried out using the Nanostring Mouse Immunology Codeset (Nanostring Technologies, Seattle, WA), comprising 561 genes. The full list of genes is shown in Supplementary Table S1. Ipsilateral hemispheres were isolated from animals perfused 5 days post-MCAO or sham operations, following the completion of the full battery of radiological and functional tests, to enable a close correlation between gene expression profiles and observed outcomes. RNA extraction was performed using the RNeasy Lipid Tissue kit (Qiagen). Analysis was conducted using the Nanostring nCounter Analysis System (Nanostring Technologies). Each reaction consisted of 250 ng of total RNA in a 5 µl aliquot, along with reporter and capture probes, six pairs of positive controls, and eight pairs of negative controls. Raw Nanostring data underwent analysis and normalization using nSolver Analysis software version 1.1 (Nanostring Technologies). Raw counts were normalized to reference gene levels as previously described [8]. One mouse was excluded from the vehicle group due to low-quality data. Gene expression data was then imported into R [30] and differentially expressed genes (DEGs) were identified using a Student's t-test with a P-value < 0.05, following established procedures [31]. The DEGs clusterograms were constructed in R using the "pheatmap" package [32].

Functional annotation

Functional annotation and interactome analysis were conducted on the DEGs using the "clusterProfiler" package for Gene Ontology (GO) biological processes and cellular components [33]. An interaction network was constructed based on gene–gene interactions sourced from the STRING database [34], which provides data on interactions among proteins or genes within species. A list of node–node interactions was acquired. Edges were then weighted based on gene co-expression data using normalized gene expression results from our study, calculated using the Weighted Gene Co-expression Network Analysis (WGCNA) algorithm[35]. The resultant network was curated and organized using Cytoscape 3.2 [36], based on node degrees (i.e. number of interactions) and edge weights (i.e. co-expression data) (Fig. 1).

Network analysis

Graph analysis was then performed to examine the network's topology using established graph theory principles first described in social networks, and recently in biological systems by our group [37–39]. This analysis was done using the "brainGraph" and "igraph" packages in R, as well as Cytoscape 3.2. Various characteristic measures of network organization were computed, including node-specific degree (k), which represents the total number of edges per node, and node strength, which is the sum of node edges' weights. Other measurements included clustering coefficient, path length, betweenness centrality, and modularity. These metrics are defined in Supplementary Table S2. We then assessed whether the resultant interaction network follows a scale-free non-random paradigm where a set of hub nodes connect peripheral nodes in the network by studying the power-law degree distributions and adjacency matrices of the networks as compared to random.

Rich-club analysis

A rich-club organization refers to a network topology in which a group of high-degree nodes, i.e. rich-club (RC), exhibit denser interconnections than what would be expected based on their individual node degrees. To quantify this phenomenon, a rich-club coefficient $\phi(k)$ is computed across the range of degrees present in the network, following the method outlined by Colizza *et. al.* [40], and optimized to protein interaction networks by our group [37, 38]. For a given degree distribution {k1, k2, …, kn}, the rich-club coefficient for each degree k is determined by calculating the ratio of the number of edges among nodes with degrees higher than k to the

maximum the possible number of edges among those nodes.

$$\phi(k) = \frac{2E_{>k}}{N_{>k}(N_{>k} - 1)}$$

where $N_{>k}$ is the number of nodes with a degree higher than k, and $E_{>k}$ is the number of edges among those nodes.

To compute the normalized rich-club coefficient, we first generated 1,000 random networks from our data. These random networks were generated to have the same degree distribution as the network under study [41]. The average rich-club coefficients for the random networks was computed and the normalized rich-club ($\rho(k)$) computed.

$$\rho(k) = \frac{\phi(k)}{\phi_{rand}(k)}$$

When the normalized rich-club coefficient $\rho(k)$ is greater than 1, it indicates the rich-club organization in the network is significant and cannot be explained by the degree distribution of the network alone. The set of nodes with $\rho(k) > 1$ were defined as the rich-club (RC).

In-silico modeling

Following the identification of the RC genes, we conducted in-silico modeling to assess upstream regulators that could serve as therapeutic targets that may influence the majority of the RC genes. This was performed using Ingenuity Pathway Analysis (IPA) [42]. Gene expression data, along with expression fold-change were used to reconstruct the network in IPA for visualization and analysis purposes. Using intrinsic IPA algorithms for the prediction of upstream regulators and downstream effects, we assessed the probable outcomes of simulated modulation (inhibition or activation) of upstream regulators on the RC genes in our network. Results of this in-silico testing were then used to guide in-vivo testing.

Principal component analysis (PCA)

To evaluate the radiographic and functional impact of DEGs within the full network and the rich-club genes, we performed PCA for dimensionality reduction. Normalized expression values were used as inputs for PCA. This elucidates the primary components that explain the variance in the data. The two or three principal components (PCs) that collectively accounted for up to 90% of the variance across all measures were selected. Subsequently, individual data points representing each animal, including stroke and sham animals, were plotted based on these selected PCs. The Eigengene, a measurement representing the eigenvector for gene expression, was then computed for each animal using PC1 and PC2. PCA and eigengene computation were performed using the "PCAtools" and "tmod" packages in R, respectively.

Statistical analysis

Statistical analyses were conducted using R and GraphPad Prism (version 10.1.1) software. The normality of distribution was assessed using the Shapiro–Wilk test. Numerical data and histograms were presented as the mean ± SD. Student's t-test (one- or two-tailed) or Mann–Whitney U test were used to compare two groups for parametric and non-parametric data, respectively, while ANOVA and Kruskal–Wallis test (KW) were employed for the analysis of more than two groups. A significance level of $P < 0.05$ was considered statistically significant. Pearson correlation coefficients were calculated to assess correlations. Proportional statistics were analyzed using the chi-square test. Fisher's exact test was employed to determine the p-value for the enrichment of annotation terms between the network and the rich-club. Generalized Linear Models (GLMs) were constructed to identify correlations between radiological, motor and cognitive outcomes, and gene expression. The eigengenes, computed from PC1 and PC2, were used as the input for gene expression of both the overall network of DEGs and rich-club genes. To compare the correlation coefficients between rich-club genes and random gene clusters, the rich-club genes correlation was compared with the averaged model-fitness of 100 random iterations of groups of DEGs, each consisting of the same number of genes as the input rich-club genes. To investigate the interaction between treatment and eigengenes for the prediction of outcomes, we used the "jtools" and "interactions" packages in R. A linear regression model was fitted with treatment and eigengenes as independent predictors and radiological, motor, or cognitive measurements as dependent outcomes. To examine the interaction effects, an interaction plot was constructed to visually represent the interaction between treatment and eigengenes on the predicted outcome. Parallel lines in the plot indicate no interaction effect, while intersecting lines indicate an interaction effect, where the effect of eigengenes on the outcome varies depending on the treatment group.

Results

Characterization of the Neuroinflammatory Gene-interaction Network after Stroke

To construct the network of neuroinflammatory gene interactions after transient MCAO, we performed targeted high-throughput gene expression analysis on the ipsilateral hemisphere of mice 5 days after undergoing sham or MCAO surgery via a Nanostring immunology gene panel (Fig. 1 and 2). A signature of

immunology-related differential expressed genes (DEGs) was identified in MCAO compared with sham animals using hierarchical clustering analysis (Fig. 2a). A full list of genes expression is provided in Supplementary Table S3. GO enrichment analysis was used to identify the prominent signaling pathways among the identified DEGs which included cytokine/chemokine signaling, leukocyte activation and migration, and complement activation (Fig. 2b).

As the focus of this work was to use disease network topology to allow for hypothesis-driven therapeutic targeting, we first constructed the interaction network among the identified DEGs using the STRING database as described in the methods (Fig. 1). The network included 181 gene nodes with a total of 4299 interactions. By studying the power-law distribution curve, the network demonstrates a clear scale-free topology exhibiting a structured arrangement characterized by the presence of central hub nodes with high connectivity and a decreasing degree of connectivity toward the network periphery (Fig. 2c,d). The network also exhibited a significantly higher clustering coefficient compared to randomly constructed networks of nodes with similar degree distribution (Fig. 2e), a finding further demonstrating the presence of small-world organization with the presence of a highway system of interactions that most nodes use to interact.

Given the presence of a small-world organization within the network, we then interrogated whether the network exhibits a rich-club organization indicating nodes that are highly interconnected with each-other and with other non-core nodes within the network. The constructed network of stroke-related DEGs exhibited a rich-club organization characterized by increased rich-club coefficient ($\phi(k)$) with increasing degree (Fig. 2f). To investigate the significance of the discovered rich-club, we assessed whether this rich-club could be explained by the degree distribution of the network using a normalized rich-club coefficient ($\rho(k)$) comparing $\phi(k)$ to that of randomly generated networks with similar degree distribution. The normalized rich-club coefficient ($\rho(k)$) reveals the presence of a significant rich-club between degrees 40 and 150 with a peak at 80 degrees (Fig. 2f). The strongest component of the rich-club was identified where the $\phi(k)$ plateaus around 1, which coincides with the highest normalized rich-club coefficient as detailed in methods. The subnetwork of nodes constituting the rich-club core is highlighted in Fig. 2g (also see Supplementary Table S3 for a list of rich-club and non-rich-club genes). Comparison of rich-club components to non-rich-club components for connectivity showed 3-fold higher degree for rich-club core genes compared to remaining nodes ($p < 0.001$) (Fig. 2h). GO analysis of the identified core genes revealed that the overall dysregulated biological processes included complement signaling pathways, cytokine-mediated signaling pathways, leukocyte proliferation, and positive regulation of leukocytic cell–cell activation and adhesion, which were also enriched in the original network (Fig. 2i).

Rich-club genes predicts radiographic outcomes

To characterize the phenotype of mice following MCAO, animals underwent MRI at day 4 after stroke to assess the extent of infarct, edema and micro-architectural changes using T2-Weighted (T2-W) imaging, DTI and DKI. T2-W imaging was used to estimate the total volume of the T2-hyperintense brain. For DTI and DKI analyses, ROIs were selected in the ischemic hippocampus and basal ganglia, and mean diffusivity (MD) and mean kurtosis (MK) were computed (see methods). Compared to sham, MCAO mice had a large area of T2-W signal hyperintensity in the ischemic territory with associated lower MD and higher MK in the designated ROIs (Fig. 3). Using linear regression analysis, the rich-club (RC) eigengenes for PC1 and 2 demonstrated a strong positive Pearson's correlation with the T2-W signal area ($R^2 = 0.57$, $P < 0.001$) that was significantly stronger than that of randomly sampled non-RC genes (Fig. 3a-b).

(See figure on next page.)

Fig. 2 Analysis of gene expression, network construction and identification of network rich-club nodes. **a** Heatmap showing the differential expression of immunology-related genes between sham (N = 4) and transient middle cerebral artery occlusion (MCAO, N = 9) groups. **b** Functional annotation for top biological processes among differentially expressed genes (DEGs) between sham and MCAO using Gene Ontology analysis. **c** Illustrative demonstration of random and scale-free network topology. **d** Curve plot showing the power law distribution of node degrees within the constructed DEGs network. **e** Bar plot showing significant difference between the clustering coefficient of the DEGs network as compared to 1000 random constructed networks with similar degree distribution. Permutation test *P < 0.01. **f** Curve plot showing the rich-club coefficient (φ) of the DEGs network (blue) and random networks (red) plotted against the left vertical axis, while normalized rich-club coefficient (ρ) (green) is plotted against right vertical axis. The gray shaded area indicated the rich-club region where $\rho > 1$, while the red shaded area indicated the strongest rich-club component where the DEGs network rich-club coefficient plateaus at $\varphi = 1$. Horizontal dashed lines correspond to φ and $\rho = 1$. **g** Interactive network showing the identified rich-club genes. **h** Bar plot showing the in degree centrality between rich-club (RC) nodes and other nodes within the DEGs network. Student's t-test. ****P < 0.001. Shown is mean ± SD **i** Functional annotation for top biological processes enriched within the rich-club genes using Gene Ontology analysis

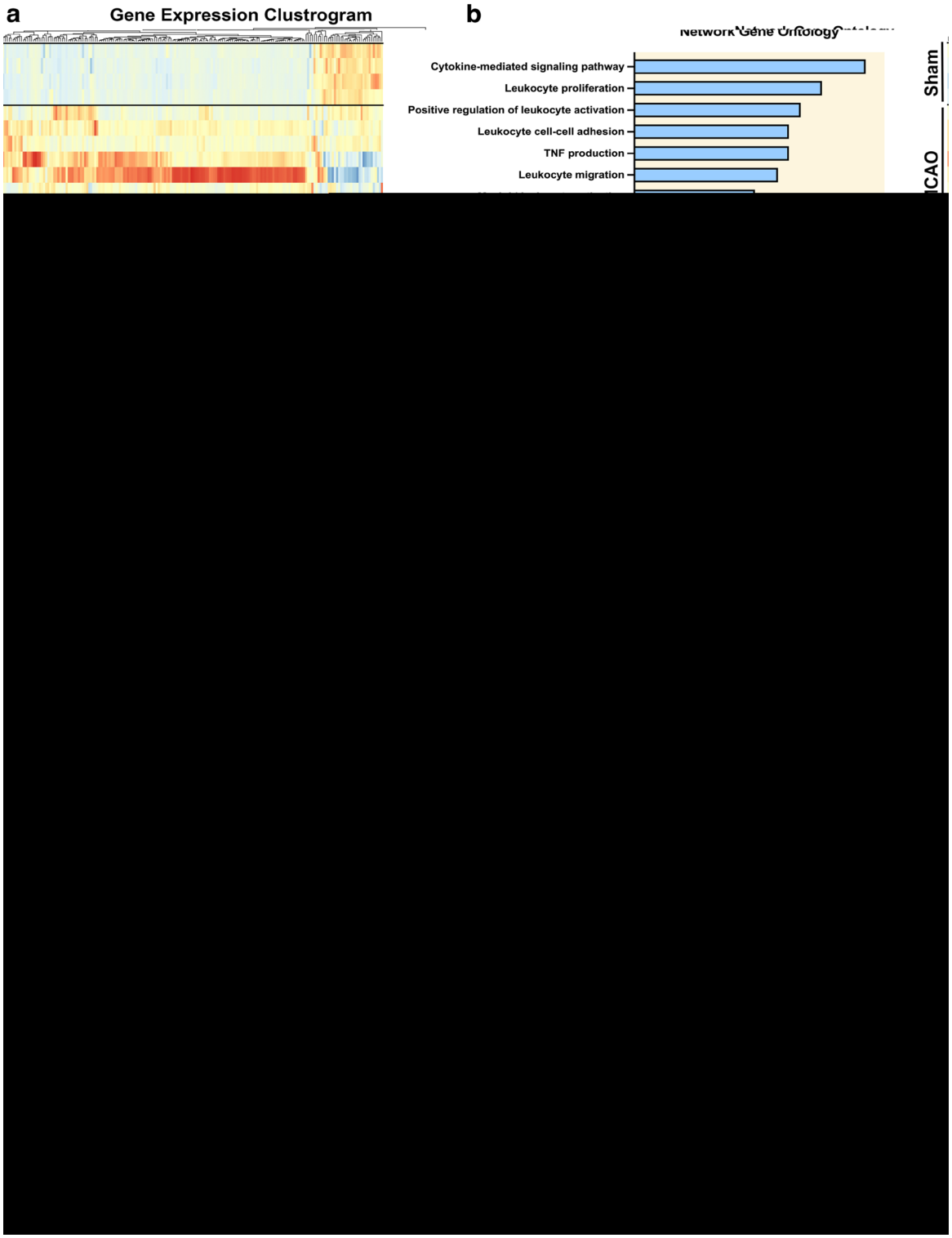

Fig. 2 (See legend on previous page.)

Similarly, the RC genes showed a stronger correlation with both MD and MK as compared to the non-RC genes with $R^2 = 0.52$ and 0.65 respectively (Fig. 3c-f). These findings indicate that the changes within the rich-club subnetwork exhibit a strong correlation with the radiographic outcomes after stroke as compared to the remaining DEG's in the network.

Rich-club Genes Predicts Behavioral Outcomes

We next performed a similar analysis evaluating the ability of RC genes to predict performance on motor tasks (NSS and corner task, Fig. 3g-l) and cognitive tasks (NOR and PA, Fig. 4a-f). The RC genes demonstrated a strong correlation with performance on motor and cognitive tasks as shown in Figs. 3 and 4 with $R^2 = 0.58$, 0.7, 0.54, and 0.7 for NSS, corner tasks, PA, and NOR tasks, respectively ($P < 0.001$, Fig. 3,4). These correlations significantly outperformed those of randomly chosen non-RC genes within the network (Fig. 3,4).

Identifying upstream regulators of the rich-club subnetwork

To identify potential therapeutic targets, we used Ingenuity Pathway Analysis (IPA) to study the upstream regulators of the rich-club subnetwork (Fig. 1). Among a total of 138 gene targets that were shown to influence the activation of at least 1 rich-club gene, the top 10 hits that targeted the highest number of rich-club genes were identified, and all of which belong to our studied panel (Supplementary Table S4). Among the top 10 hits, only Amyloid Precursor protein (APP) and C3 showed significant dysregulation in our network when comparing MCAO to sham (Supplementary table S4); APP was downregulated in MCAO and C3 was upregulated. Given that the complement pathway plays a pivotal role in the neuroinflammatory response following a stroke, and that site-targeted inhibitory approaches for C3 activation are in clinical development (namely CR2-fH and its human equivalents [8, 19, 43, 44]), we simulated the effect of C3 inhibition on the RC subnetwork. C3 directly interacted with 27 genes within the full network of DEG in MCAO versus sham and with 10 genes within the rich-club subnetwork (30%), and indirectly interacted with all rich-club genes (Fig. 5a) leading to downregulation of all but one gene (TP53) with simulated inhibition of C3. Functional annotation of direct C3 targets within the rich-club subnetwork revealed regulation of biological processes, including chemokine activity, immune cells chemotaxis, and TNF production. In the broader neuroinflammatory network, C3 targets were associated with processes such as humoral immune responses, and leukocyte migration and activation (Supplementary Fig. 1).

Inhibition of C3 favorably reverses rich-club gene alterations after MCAO and improves outcomes

Based on this *in-silico* model, we performed in-vivo testing using the same MCAO murine model while administering either vehicle (phosphate buffered saline) or CR2-fH at 2 h after reperfusion via tail vein injection while performing the same battery of radiographic, behavioral, and transcriptional studies. CR2-fH significantly reversed the eigengene changes seen in the vehicle group in direction toward the sham (Fig. 5b), and significantly reversed the expression of 36% of the rich-club genes (based on $P < 0.05$, Student's t-test) (Fig. 5c,d), thus supporting the expected findings from our *in-silico* model (Fig. 5a). Using PCA, the 3 PC for the rich-club genes demonstrated clear clustering of the different treatment groups including sham, vehicle and CR2-fH, where CR2-fH demonstrates migration of the cohort away from the vehicle and closer to the sham group (Fig. 6a). We then evaluated the impact of CR2-fH on the different outcome measures using linear regression models testing the effect of CR2-fH as compared to vehicle as reference on each outcome measure while reporting the model estimates for CR2-fH (Fig. 6b). Except for MD on DTI, CR2-fH significantly predicted all radiographic and behavioral outcomes including T2-W signal area, MK, NSS, and performance on corner, passive avoidance and NOR tasks (Fig. 6b). To determine if the alterations in the rich-club genes explained the impact of CR2-fH on these outcome measures, we performed interaction analyses within these models to test whether the eigengenes for rich-club genes showed significant interaction with the impact of CR2-fH on outcomes (Fig. 6c). Results of interaction analyses showed robust interactions with respect

(See figure on next page.)

Fig. 3 Rich-club genes predicts radiographic and motor outcomes. Illustration of T2-Weighted (T2-W) and diffusion tensor imaging (DTI) from animals undergoing sham or MCAO operations. Red fields denote areas of ROI for mean diffusivity (MD) and MK calculations. **a**–**f** Radiographic outcomes: Linear regression models predicting **a** MRI T2-signal area **c** MD, and **e** diffuse kurtosis imaging (DKI). Reported values are Pearson's R^2 and P-value. **b**, **d**, **f** Bar plots showing significant difference between the regression model R^2 for the prediction of **b** T2-signal **d** DTI, **f** DKI between the RC genes versus 100 random iterations of non-RC genes. One-sample t-test. *$P < 0.05$. **g**-**l** Motor outcomes: **g** comparison of NSS between sham and MCAO mice at day 3. Mann–Whitney U test. ***$P < 0.001$. **h** Linear regression model predicting performance on NSS based on RC PC1 and 2 eigengenes. **i** Bar plot showing significant difference between the regression model R^2 for the prediction of NSS between the RC genes versus 100 random iterations of non-RC genes. One-sample t-test. *$P < 0.05$. **j** comparison of forearm asymmetry on corner task between sham and MCAO mice at day 4. Mann–Whitney U test. ***$P < 0.001$. **h** Linear regression model predicting performance on corner task based on RC PC1 and 2 eigengenes. **i** Bar plot showing significant difference between the regression model R^2 for the prediction of corner task between the RC genes versus 100 random iterations of non-RC genes. One-sample t-test. *$P < 0.05$. All bar plots show mean ± SD

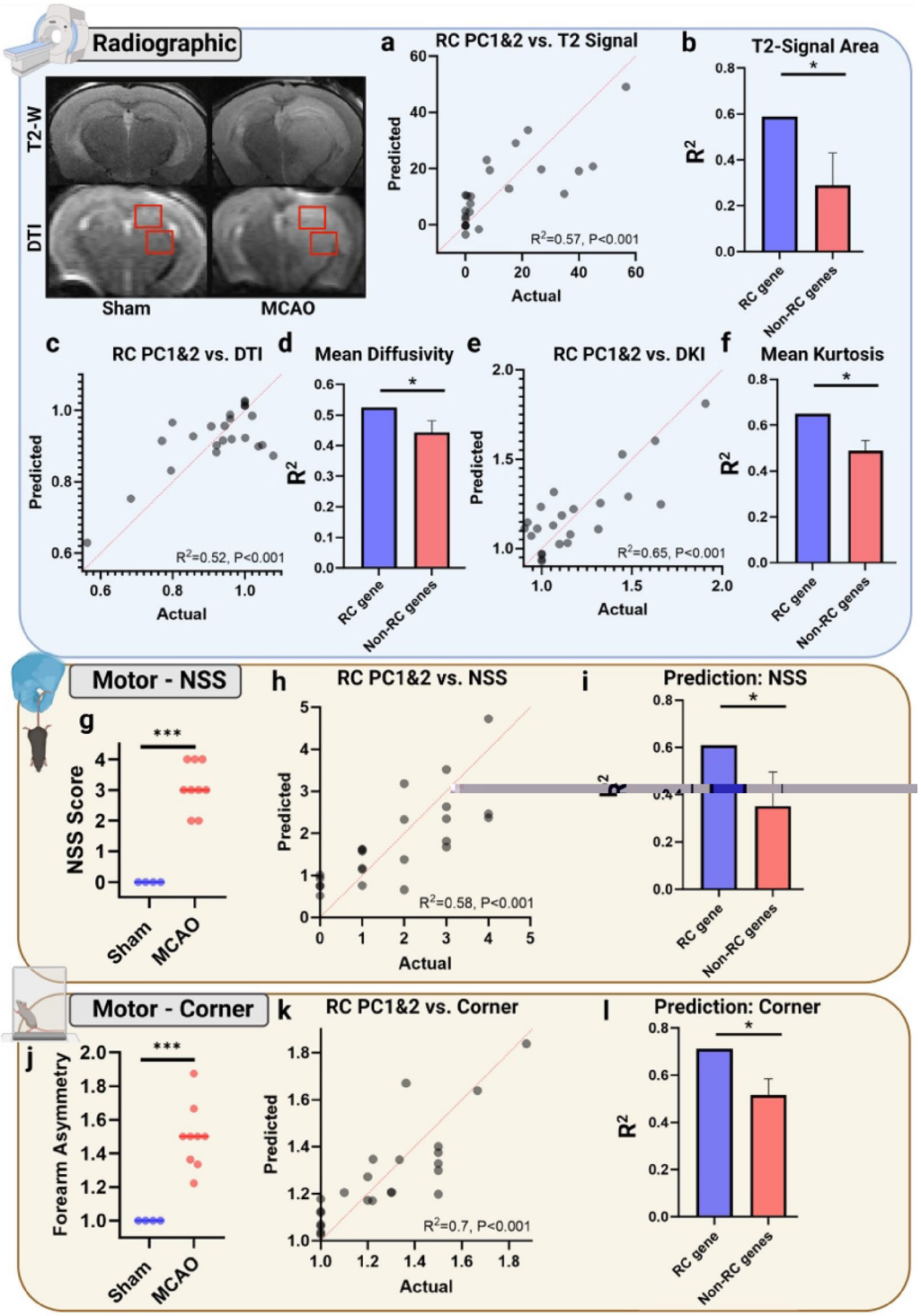

Fig. 3 (See legend on previous page.)

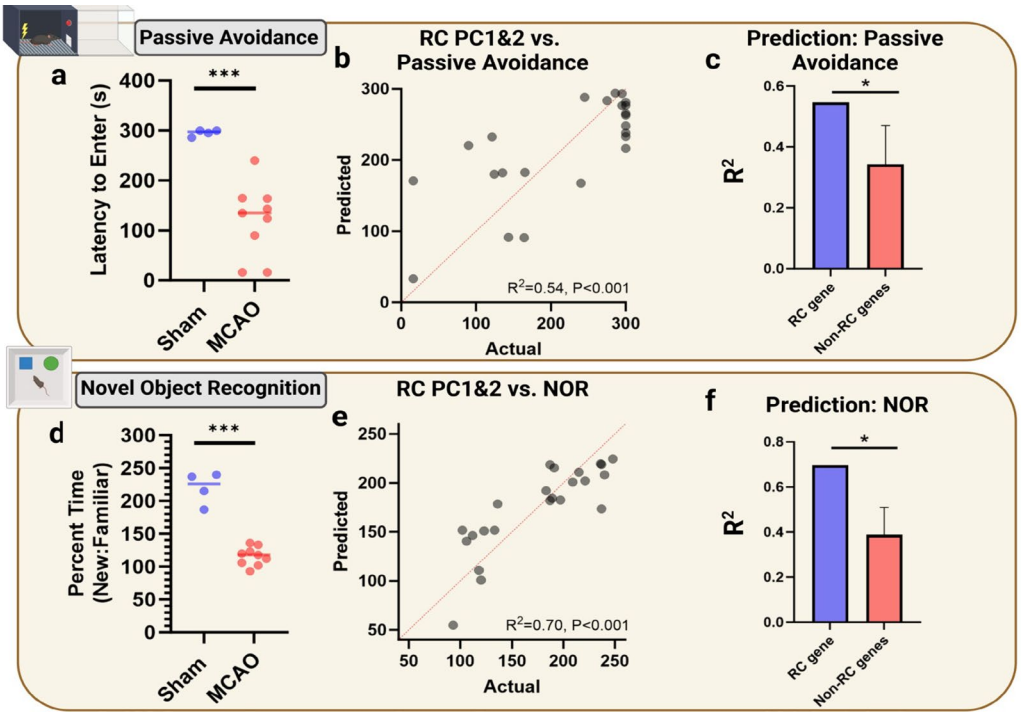

Fig. 4 Rich-club genes predict cognitive outcomes. **a** Comparison of latency to enter the dark box on passive avoidance task between sham and MCAO mice at day 4. Student's t-test. ***P < 0.001. **b** Linear regression model predicting performance on passive avoidance based on RC PC1 and 2 eigengenes. **c** Bar plot showing significant difference between the regression model R^2 for the prediction of passive avoidance performance between the RC genes versus 100 random iterations of non-RC genes. One-sample t-test. *P < 0.05. **d** Comparison of novel object recognition (NOR) performance between sham and MCAO mice at day 3. Student's t-test. ***P < 0.001. **e** Linear regression model predicting performance on NOR task based on RC PC1 and 2 eigengenes. **f** Bar plot showing significant difference between the regression model R^2 for the prediction of NOR task between the RC genes versus 100 random iterations of non-RC genes. One-sample t-test. *P < 0.05. All bar plots show mean ± SD

to all outcome measures. These findings suggest that targeting C3 activation using CR2-fH improved functional and behavioral outcomes after stroke by influencing a core subnetwork of neuroinflammatory rich-club genes.

Discussion

In this work, we develop an analytical framework of combining transcriptomics, graph theory applications, in-silico testing, and in-vivo validation to study the molecular underpinning of the post-ischemic neuroinflammatory response and its potential therapeutic modulation. We constructed a network of neuroinflammatory gene interactions following transient MCAO that revealed a scale-free topology with a rich-club organization. This rich-club consisted of key regulatory genes that were highly interconnected, forming a core network critical to the neuroinflammatory response. The presence of a rich-club organization in our network indicates a hierarchical structure where a few hub genes exert substantial control over the network's functionality, supporting the hypothesis that these hubs could be strategic targets for therapeutic intervention. In the realm of cellular biology, the application of graph theory concepts, particularly scale-free network topology, has significantly advanced our understanding of protein–protein interactions by revealing network organization. Scale-free networks, recognized as the fundamental topology of biological networks, exhibit an uneven distribution of nodes, with some nodes displaying higher connectivity and influence. Identifying these nodes is crucial for comprehending disease pathophysiology and pinpointing effective drug targets [40, 45, 46].

Rich-club analysis, a concept in graph theory, is employed to identify core nodes within a network. This analysis capitalizes on the tendency of a subset of nodes within a scale-free network to form a 'club' characterized by high interconnectivity [40, 45, 46]. This organizational structure serves two fundamental functions. Firstly, it facilitates rapid signal transmission among club members due to their high connectivity. Secondly, it creates a robust resilient network wherein the loss of a rich-club node can be compensated for by signal propagation from other club members, minimizing disruption to the overall network. Another key aspect of rich-club organization is that these highly connected nodes not only interact strongly with each other but also with fewer central nodes

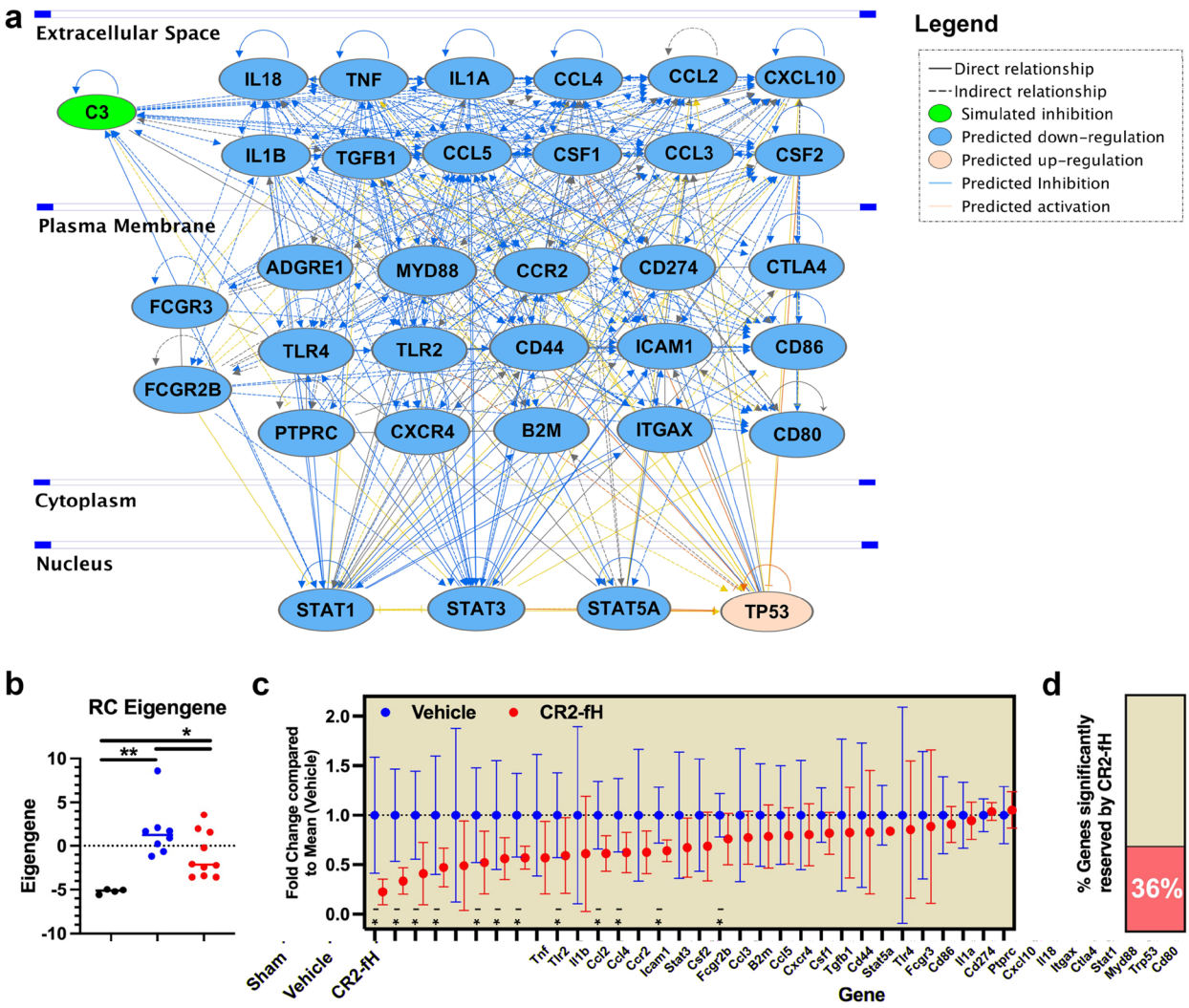

Fig. 5 Identifying and targeting C3 as an upstream regulator of the rich-club subnetwork. **a** In-silico analysis showing the simulated effect of C3 inhibition on the expression of rich-club genes. Analysis was done using Ingenuity Pathway Analysis (IPA) software. **b** Dot plot showing the difference in rich-club genes eigengene between sham (N = 4), vehicle (N = 8), and CR2-fH treatment (N = 10) groups. ANOVA with Holm-Sidak's test for multiple comparisons. *P < 0.05. **P < 0.01. One data point in the vehicle group with a value of 17.8 was identified as an outlier using Grubbs' test (G = 2.4, α = 0.05) and excluded from this analysis. **c** Dot plot showing the expression of individual rich-club genes between treatment groups. Shown is mean ± SD. *P < 0.05. **d** Bar plot showing the percentage of genes with significantly reversed expression between both treatment groups based on P < 0.05 on Student's t-test

within the network, ensuring efficient signal propagation across the network. Initially, such organization poses a challenge, particularly in disease pathology, as inhibiting a pathological network may seem intractable. However, leveraging the organizational power of the rich-club is key. Drugs targeting a majority of rich-club nodes can harness the high connectivity within the club, allowing it to propagate the therapeutic effect to other core nodes of the network. Additionally, the rich-club's extensive connectivity with the rest of the network ensures the spread of the therapeutic effect throughout the entire network, exerting a widespread impact [38, 40, 45].

Previous work using different molecular datasets and data mining strategies has studied the network of dysregulated genes after ischemic stroke[38, 47–49]. These studies focused on identifying gene interaction network modules and performed enrichment analysis for prominent pathways and genes in the network. A scale-free network of gene interactions was described and emphasized the role of inflammatory cytokines and chemotactic signaling pathways which overlap with the findings of

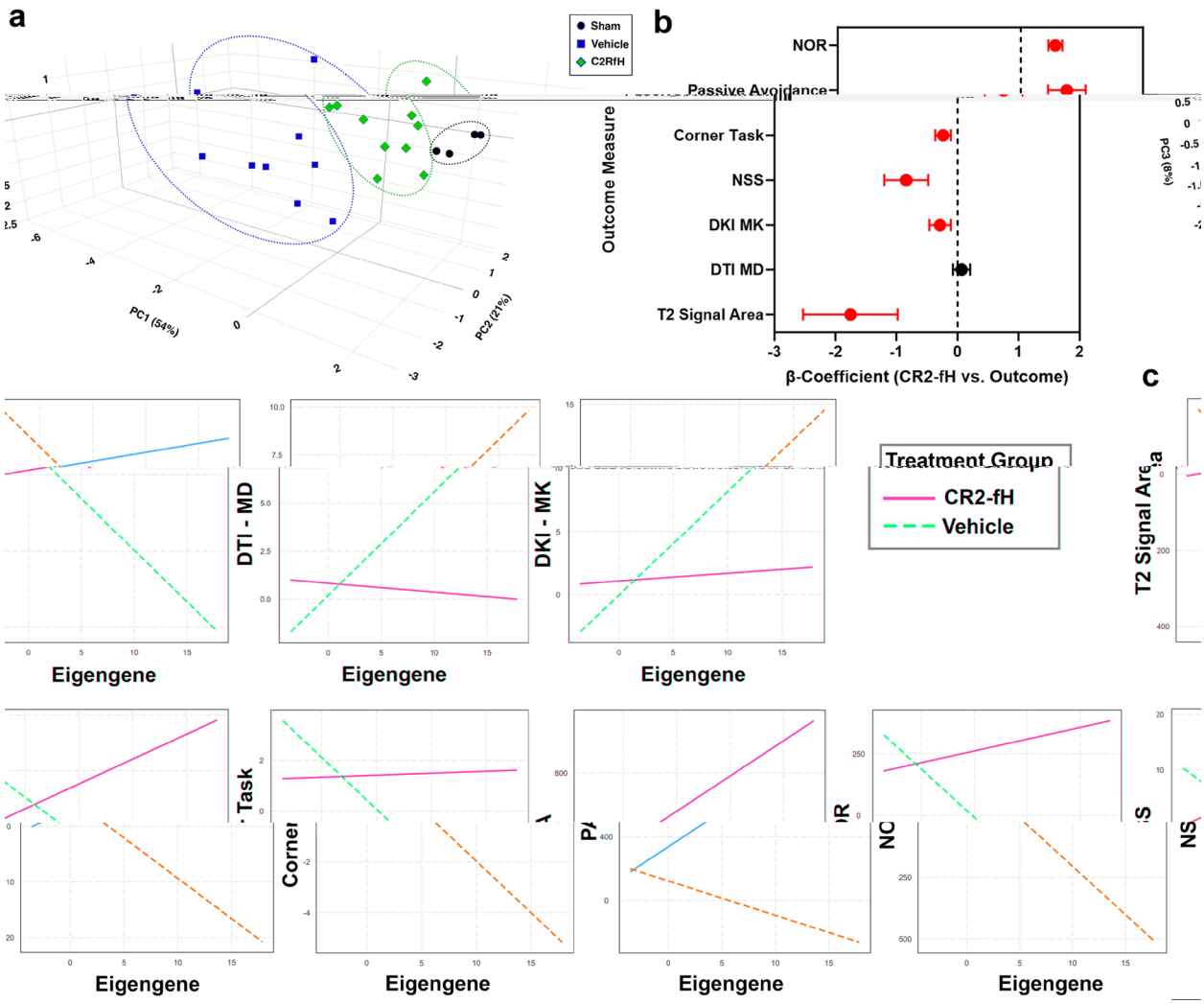

Fig. 6 The interactive effect between rich-club genes expression and treatment on outcomes. **a** Principal component analysis (PCA) 3-dimentional plot using differentially clustering of treatment groups based on rich-club genes eigengene. **b** Results of linear regression models using treatment group (CR2-fH) versus vehicle as reference to predict radiographic and behavioral outcomes. Shown are standardized estimates with 95% confidence intervals. Red highlights the variables where CR2-fH significantly predicted performance. **c** Fitted linear regression model interactive plot with treatment and eigengenes as independent predictors and radiological, motor, or cognitive measurements as dependent outcomes. Parallel lines in the plot indicate no interaction effect, while intersecting lines indicate an interaction effect, where the effect of eigengenes on the outcome varies depending on the treatment group. All outcome measures showed significant interaction between the eigengene value and the effect of CR2-fH on outcome measures. DTI-MD, diffusion tensor imaging—mean diffusivity; DKI-MK, diffusion kurtosis imaging—mean kurtosis; NSS, neurological severity score; PA, passive avoidance; NOR, novel object recognition task

this study [47–49]. In prior work from our group using curated protein expression data from published reports, a rich-club organization was identified with a similar pattern of enriched inflammatory activation pathways, including immune cell activation, chemotaxis, and adhesion [38]. However, the correlates of these findings with functional outcomes had not been investigated. In this work, we demonstrated that rich-club genes, identified through graph theory-based network analysis, showed strong correlations with both radiographic and functional outcomes that significantly outperformed those of differentially expressed non-rich-club genes. This suggests that the rich-club genes play pivotal roles in pathological processes following ischemic stroke, influencing both structural and behavioral manifestations of injury. Specifically, the eigengene for rich-club genes exhibited a robust positive correlation with T2-weighted imaging (T2-W) signal area, mean diffusivity (MD), and mean kurtosis (MK) metrics from diffusion tensor imaging (DTI) and diffusion kurtosis imaging (DKI). These correlations

underscore the importance of rich-club genes in mediating the extent of ischemic damage and subsequent tissue remodeling.

The functional significance of the rich-club was further highlighted by the strong correlation of these genes with motor and cognitive outcomes in MCAO mice. The rich-club eigengene demonstrated a significant association with neurological severity scores (NSS), corner task performance, passive avoidance (PA), and novel object recognition (NOR) tasks. These behavioral assessments reflect both sensorimotor and cognitive deficits, which are critical determinants of long-term recovery post-stroke. The superior predictive power of rich-club genes over randomly selected DEGs underscores their central role in orchestrating post-stroke pathology. The rich-club genes identified involve extracellular secretory cytokines and chemotactic factors, membrane-bound phagocytic and antigen recognition markers, and transcriptional regulators of the Jak/STAT signaling pathway. Given that these components cannot be targeted by single agents, we interrogated upstream regulators that can preferentially influence the rich-club genes.

In exploring upstream regulators of the rich-club subnetwork, among the top 10 regulators, only C3 and APP were significantly differentially expressed in vivo, with C3 upregulated and APP downregulated. Although in-silico analysis indicated an activator role for APP within the RC subnetwork (Supplementary Fig. 2), its overall downregulation in the stroke group compared to the sham group suggested it is unlikely to be a primary driver of pathology in this context. APP does play a significant role in driving pathology neurodegenerative neuroinflammation in stroke as well as neurodegenerative disease mainly due to the pathological accumulation of A-beta peptides [50–52]. However, investigating the protein breakdown pattern of APP falls beyond the scope of our work. In contrast, C3 was upregulated in the stroke group and appeared to serve as a key driver of the RC subnetwork. C3 dysregulation in the MCAO model, is consistent with its known role in stroke-induced neuroinflammation. Several prior reports on analysis of clinical samples and preclinical investigations have emphasized an important role for complement activation in the pathology of ischemic stroke, and complement inhibitors have been investigated in preclinical models and early clinical phases for treatment of exacerbated neuroinflammation after injury [6–8, 15, 19, 21–23]. The complement system serves as both a recognition and effector system of innate immunity that recognizes early danger-related signals and is capable of activating a wide range of innate and adaptive immune mechanisms [15, 17, 18, 20]. Using in-silico modeling, we predicted that inhibition of C3 would downregulate the majority of rich-club genes, suggesting a broad modulatory effect on the neuroinflammatory network. This hypothesis was tested in vivo using a recombinant fusion protein, CR2-fH, designed to specifically inhibit the alternative pathway of complement activation at the C3 activation step. CR2-fH is a fusion protein consisting of a fragment of complement receptor 2 (CR2) that binds to tissue-bound C3 activation products (C3b/iC3b/C3d), linked to an active portion of the complement inhibitor factor H (fH) [16, 19]. Previous studies have demonstrated that CR2-fH, through targeted complement inhibition of the alternative pathway, provides neuroprotection following ischemic stroke in rodent models [8, 19, 53]. This neuroprotective effect includes modulation of gliosis and microglial activation, and reduction of cellular apoptosis [6, 8, 19, 29, 43, 53]. However, the detailed pathophysiology remains unclear. Therefore, we investigated how CR2-fH treatment in the same rodent model impacts rich-club gene expression and functional outcomes. Treatment with CR2-fH significantly reversed the expression of rich-club genes, aligning with our in-silico predictions. Functional annotation of C3 targets indicates that CR2-fH reduced leukocyte chemotaxis to the injury site and limited leukocyte activation. This suppressed the initiation of both innate and adaptive immune responses, mitigating the neuroinflammatory cascade after stroke. Furthermore, CR2-fH treatment improved both radiographic and functional outcomes. The interaction analyses confirmed that the impact of CR2-fH on these outcomes was mediated through its effect on rich-club genes. These findings highlight the therapeutic potential of targeting central nodes within the neuroinflammatory network, offering a strategy to mitigate secondary injury following stroke. The integration of graph theory with experimental neurobiology in this study provides a novel framework for identifying and validating therapeutic targets in complex disease networks. Another added advantage of this study is its alignment with the latest STAIR recommendations for testing neuroprotective agents within the context of reperfusion therapy, the current standard of care [54]. Additionally, cross-sectional in-vivo imaging was utilized for lesion analysis using sequences similar to those employed in clinical settings.

Our study underscores the significance of neuroinflammation in stroke pathology and recovery, emphasizing the need for multifaceted therapeutic approaches that address the complexity of the post-stroke inflammatory response. By focusing on key regulatory hubs within the neuroinflammatory network, we demonstrate the feasibility of network-based therapeutic targeting, paving the way for more effective interventions in stroke care. Future research should continue to explore the dynamic interactions within neuroinflammatory networks and their modulation by therapeutic agents, with the goal of improving clinical outcomes for stroke patients. Finally,

our investigation strategy provides a platform to leverage in-silico modeling and network analysis to guide translational research, an approach that could be applied to a wide range of disease processes.

Limitations

The study involved gene expression analysis using the Nanostring Immunology panel rather than a full transcriptomic analysis which limits the ability to assess the contribution of non-inflammatory genes to the overall dysregulation networks. However, when compared to previously published interaction networks for brain ischemia, the majority of key hub genes were part of our panel[38]. The detailed effect of CR2-fH on clinical pathology and outcomes after murine stroke including acute and chronic outcomes have been previously investigated, including its impact on gene expression profiles [8, 19], but this work uses data curated from these studies and additional experiments to study how that effect modulates network-level biology and how network-level organization impact different radiographic, motor and cognitive outcomes.

Supplementary Information

The online version contains supplementary material available at https://doi.org/10.1186/s12974-024-03316-z.

Supplementary material 1: Supplementary Figure 1. Functional annotation of C3 targets within the neuroinflammatory network. Functional annotation for top biological processes among the C3 targets within (a) the rich-club (RC) subnetwork and (b) the full neuroinflammatory network using Gene Ontology (GO) analysis.

Supplementary material 2: Supplementary Figure 2. In-silico analysis showing the simulated effect of APP upregulation on the expression of rich-club genes. Analysis was done using Ingenuity Pathway Analysis (IPA) software.

Supplementary material 3.

Supplementary material 4.

Supplementary material 5.

Supplementary material 6.

Acknowledgements
None.

Disclosures
Ali Alawieh and Stephen Tomlinson are inventors of a US patent on the use of targeted complement inhibitors in neurological disorders.

Author contributions
YMZ and AMA led this project and were involved in all aspects of the project. AMA supervised all the mouse surgieres and functional outcomes tests. YMZ wrote the code needed for the analysis. FHK and ST helped with data analyses. YMZ and AMA wrote the initial manuscript draft. TGM, JAG, DLB, BMH and GP supervied this project and reviewed and edited the manuscript.

Funding
This work was supported by Emory Department of Neurosurgery Catalyst Grant (AA and JG), Emory Medical Care Foundation (EMCF) Grant (AA and JG), Department of Veterans Affairs Merit Awards 1BX004256, 1RX001141, 21RX002363, and IK6BX005235 (ST and AA), and American Heart Association Fellowship Grant 15PRE25250009 (AA).

Data availability
All data included in the submission.

Declarations

Ethics approval and consent to participate
Not applicable.

Competing interests
The authors declare no competing interests.

Author details
[1]Department of Neurosurgery, Emory University School of Medicine, Atlanta, GA 30322, USA. [2]Department of Neurobiology, Morehouse School of Medicine, Atlanta, GA, USA. [3]Department of Microbiology and Immunology, Medical University of South Carolina, Charleston, SC, USA. [4]Ralph Johnson VA Medical Center, Charleston, SC, USA.

Received: 29 September 2024 Accepted: 29 November 2024
Published online: 04 January 2025

References

1. Albers GW, Marks MP, Kemp S, et al. Thrombectomy for stroke at 6 to 16 hours with selection by perfusion imaging. N Engl J Med. 2018;378(8):708–18. https://doi.org/10.1056/NEJMoa1713973.
2. Albers GW, Marks MP, Lansberg MG. Thrombectomy for stroke with selection by perfusion imaging. N Engl J Med. 2018;378(19):1849–50. https://doi.org/10.1056/NEJMc1803856.
3. Jovin TG, Chamorro A, Cobo E, et al. Thrombectomy within 8 hours after symptom onset in ischemic stroke. N Engl J Med. 2015;372(24):2296–306. https://doi.org/10.1056/NEJMoa1503780.
4. Jovin TG, Nogueira RG, Investigators D. Thrombectomy 6 to 24 hours after stroke. N Engl J Med. 2018;378(12):1161–2. https://doi.org/10.1056/NEJMc1801530.
5. Saver JL, Goyal M, Bonafe A, et al. Stent-retriever thrombectomy after intravenous t-PA vs. t-PA alone in stroke. N Engl J Med. 2015;372(24):2285–95. https://doi.org/10.1056/NEJMoa1415061.
6. Alawieh A, Langley EF, Tomlinson S. Targeted complement inhibition salvages stressed neurons and inhibits neuroinflammation after stroke in mice. Sci Transl Med. 2018. https://doi.org/10.1126/scitranslmed.aao6459.
7. Alawieh A, Langley F, Tomlinson S. The inflammatory response and its effect on rehabilitation-induced repair processes after stroke. *Cellular and molecular approaches to regeneration and repair* 2018:509–520.
8. Alawieh A, Andersen M, Adkins DL, Tomlinson S. Acute complement inhibition potentiates neurorehabilitation and enhances tPA-mediated neuroprotection. J Neurosci. 2018;38(29):6527–45. https://doi.org/10.1523/JNEUROSCI.0111-18.2018.
9. Alawieh AM, Langley EF, Feng W, Spiotta AM, Tomlinson S. Complement-dependent synaptic uptake and cognitive decline after stroke and reperfusion therapy. J Neurosci. 2020;40(20):4042–58. https://doi.org/10.1523/JNEUROSCI.2462-19.2020.
10. Goyal M, Menon BK, van Zwam WH, et al. Endovascular thrombectomy after large-vessel ischaemic stroke: a meta-analysis of individual patient data from five randomised trials. Lancet. 2016;387(10029):1723–31. https://doi.org/10.1016/S0140-6736(16)00163-X.
11. Hernandez-Jimenez M, Abad-Santos F, Cotgreave I, et al. APRIL: A double-blind, placebo-controlled, randomized, Phase Ib/IIa clinical study of ApTOLL for the treatment of acute ischemic stroke. Front Neurol. 2023;14:1127585. https://doi.org/10.3389/fneur.2023.1127585.
12. Lyden P, Pryor KE, Coffey CS, et al. Final results of the RHAPSODY trial: a multi-center, phase 2 trial using a continual reassessment method to determine the safety and tolerability of 3K3A-APC, a recombinant variant of human activated protein C, in combination with tissue plasminogen activator, mechanical thrombectomy or both in moderate to severe

acute ischemic stroke. Ann Neurol. 2019;85(1):125–36. https://doi.org/10.1002/ana.25383.
13. Hill MD, Goyal M, Menon BK, et al. Efficacy and safety of nerinetide for the treatment of acute ischaemic stroke (ESCAPE-NA1): a multicentre, double-blind, randomised controlled trial. Lancet. 2020;395(10227):878–87. https://doi.org/10.1016/S0140-6736(20)30258-0.
14. Couch C, Alawieh AM, Toutonji A, Atkinson C, Tomlinson S. Evaluating the comorbidities of age and cigarette smoking on stroke outcomes in the context of anti-complement mitigation strategies. Front Immunol. 2023;14:1161051. https://doi.org/10.3389/fimmu.2023.1161051.
15. Alawieh A, Elvington A, Tomlinson S. Complement in the homeostatic and ischemic brain. Front Immunol. 2015;6:417. https://doi.org/10.3389/fimmu.2015.00417.
16. Alawieh A, Tomlinson S. Injury site-specific targeting of complement inhibitors for treating stroke. Immunol Rev. 2016;274(1):270–80. https://doi.org/10.1111/imr.12470.
17. Dalakas MC, Alexopoulos H, Spaeth PJ. Complement in neurological disorders and emerging complement-targeted therapeutics. Nat Rev Neurol. 2020;16(11):601–17. https://doi.org/10.1038/s41582-020-0400-0.
18. Schartz ND, Tenner AJ. The good, the bad, and the opportunities of the complement system in neurodegenerative disease. J Neuroinflammation. 2020;17(1):354. https://doi.org/10.1186/s12974-020-02024-8.
19. Alawieh A, Elvington A, Zhu H, et al. Modulation of post-stroke degenerative and regenerative processes and subacute protection by site-targeted inhibition of the alternative pathway of complement. J Neuroinflamm. 2015;12:247. https://doi.org/10.1186/s12974-015-0464-8.
20. Alawieh A, Narang A, Tomlinson S. Complementing regeneration. Oncotarget. 2015;6(26):21769–70. https://doi.org/10.18632/oncotarget.4844.
21. Huang J, Kim LJ, Mealey R, et al. Neuronal protection in stroke by an sLex-glycosylated complement inhibitory protein. Science. 1999;285(5427):595–9. https://doi.org/10.1126/science.285.5427.595.
22. Ma Y, Liu Y, Zhang Z, Yang GY. Significance of complement system in ischemic stroke: a comprehensive review. Aging Dis. 2019;10(2):429–62. https://doi.org/10.14336/AD.2019.0119.
23. Pedersen ED, Waje-Andreassen U, Vedeler CA, Aamodt G, Mollnes TE. Systemic complement activation following human acute ischaemic stroke. Clin Exp Immunol. 2004;137(1):117–22. https://doi.org/10.1111/j.1365-2249.2004.02489.x.
24. Alawieh A, Wang W, Narang A, Tomlinson S. Thromboembolic model of cerebral ischemia and reperfusion in mice. Methods Mol Biol. 2016;1462:357–72. https://doi.org/10.1007/978-1-4939-3816-2_20.
25. Tabesh A, Jensen JH, Ardekani BA, Helpern JA. Estimation of tensors and tensor-derived measures in diffusional kurtosis imaging. Magn Reson Med. 2011;65(3):823–36. https://doi.org/10.1002/mrm.22655.
26. Mallah K, Couch C, Alshareef M, et al. Complement mediates neuroinflammation and cognitive decline at extended chronic time points after traumatic brain injury. Acta Neuropathol Commun. 2021;9(1):72. https://doi.org/10.1186/s40478-021-01179-6.
27. Zhang L, Schallert T, Zhang ZG, et al. A test for detecting long-term sensorimotor dysfunction in the mouse after focal cerebral ischemia. J Neurosci Methods. 2002;117(2):207–14. https://doi.org/10.1016/s0165-0270(02)00114-0.
28. Alawieh A, Chalhoub RM, Mallah K, et al. Complement drives synaptic degeneration and progressive cognitive decline in the chronic phase after traumatic brain injury. J Neurosci. 2021;41(8):1830–43. https://doi.org/10.1523/JNEUROSCI.1734-20.2020.
29. Huang Y, Qiao F, Atkinson C, Holers VM, Tomlinson S. A novel targeted inhibitor of the alternative pathway of complement and its therapeutic application in ischemia/reperfusion injury. J Immunol. 2008;181(11):8068–76. https://doi.org/10.4049/jimmunol.181.11.8068.
30. R Core Team R. R: a language and environment for statistical computing. 2013;
31. Geiss GK, Bumgarner RE, Birditt B, et al. Direct multiplexed measurement of gene expression with color-coded probe pairs. Nat Biotechnol. 2008;26(3):317–25. https://doi.org/10.1038/nbt1385.
32. Kolde R. Pheatmap: pretty heatmaps. R package version 1.0. 12. 2019.
33. Yu G, Wang LG, Han Y, He QY. clusterProfiler: an R package for comparing biological themes among gene clusters. OMICS. 2012;16(5):284–7. https://doi.org/10.1089/omi.2011.0118.
34. Mering CV, Huynen M, Jaeggi D, Schmidt S, Bork P, Snel B. STRING: a database of predicted functional associations between proteins. Nucleic Acids Res. 2003;31(1):258–61.
35. Langfelder P, Horvath S. WGCNA: an R package for weighted correlation network analysis. BMC Bioinf. 2008;9:1–13.
36. Kohl M, Wiese S, Warscheid B. Cytoscape: software for visualization and analysis of biological networks. Data mining in proteomics: from standards to applications 2011:291–303.
37. Alawieh A, Sabra M, Sabra Z, Tomlinson S, Zaraket FA. Molecular architecture of spinal cord injury protein interaction network. PLoS ONE. 2015;10(8): e0135024. https://doi.org/10.1371/journal.pone.0135024.
38. Alawieh A, Sabra Z, Sabra M, Tomlinson S, Zaraket FA. A rich-club organization in brain ischemia protein interaction network. Sci Rep. 2015;5:13513. https://doi.org/10.1038/srep13513.
39. Sabra M, Alawieh A, Zaraket FA. Intractome curation and analysis for stroke and spinal cord injury using semiautomatic annotations. Leveraging Biomedical and Healthcare Data. Elsevier; 2019:151–166.
40. Colizza V, Flammini A, Serrano MA, Vespignani A. Detecting rich-club ordering in complex networks. Nat Phys. 2006;2(2):110–5.
41. Viger F, Latapy M. Efficient and simple generation of random simple connected graphs with prescribed degree sequence. J Complex Netw. 2016;4(1):15–37.
42. Kramer A, Green J, Pollard J Jr, Tugendreich S. Causal analysis approaches in ingenuity pathway analysis. Bioinformatics. 2014;30(4):523–30. https://doi.org/10.1093/bioinformatics/btt703.
43. Liu F, Ryan ST, Fahnoe KC, et al. C3d-Targeted factor H inhibits tissue complement in disease models and reduces glomerular injury without affecting circulating complement. Mol Ther. 2024;32(4):1061–79. https://doi.org/10.1016/j.ymthe.2024.02.001.
44. Risitano AM, Notaro R, Pascariello C, et al. The complement receptor 2/factor H fusion protein TT30 protects paroxysmal nocturnal hemoglobinuria erythrocytes from complement-mediated hemolysis and C3 fragment opsonization. Blood J Am Soc Hematol. 2012;119(26):6307–16.
45. Wuchty S. Rich-club phenomenon in the interactome of P. falciparum--artifact or signature of a parasitic life style? *PLoS One.* 2007;2(3):e335. https://doi.org/10.1371/journal.pone.0000335
46. Aloy P, Russell RB. Taking the mystery out of biological networks. EMBO Rep. 2004;5(4):349–50. https://doi.org/10.1038/sj.embor.7400129.
47. Quan Z, Quan Y, Wei B, et al. Protein-protein interaction network and mechanism analysis in ischemic stroke. Mol Med Rep. 2015;11(1):29–36. https://doi.org/10.3892/mmr.2014.2696.
48. Zhang L, Liu B, Han J, Wang T, Han L. Competing endogenous RNA network analysis for screening inflammation-related long non-coding RNAs for acute ischemic stroke. Mol Med Rep. 2020;22(4):3081–94. https://doi.org/10.3892/mmr.2020.11415.
49. Hu W, Li P, Zeng N, Tan S. Exploring the hub mechanisms of ischemic stroke based on protein-protein interaction networks related to ischemic stroke and inflammatory bowel disease. Sci Rep. 2023;13(1):1741. https://doi.org/10.1038/s41598-023-27459-w.
50. Goulay R, Mena Romo L, Hol EM, Dijkhuizen RM. From stroke to dementia: a comprehensive review exposing tight interactions between stroke and amyloid-beta formation. Transl Stroke Res. 2020;11(4):601–14. https://doi.org/10.1007/s12975-019-00755-2.
51. Hampel H, Hardy J, Blennow K, et al. The amyloid-beta pathway in Alzheimer's disease. Mol Psychiatry. 2021;26(10):5481–503. https://doi.org/10.1038/s41380-021-01249-0.
52. O'Brien RJ, Wong PC. Amyloid precursor protein processing and Alzheimer's disease. Annu Rev Neurosci. 2011;34:185–204. https://doi.org/10.1146/annurev-neuro-061010-113613.
53. Elvington A, Atkinson C, Zhu H, et al. The alternative complement pathway propagates inflammation and injury in murine ischemic stroke. J Immunol. 2012;189(9):4640–7. https://doi.org/10.4049/jimmunol.1201904.
54. Wechsler LR, Adeoye O, Alemseged F, et al. Most promising approaches to improve stroke outcomes: the stroke treatment academic industry roundtable XII workshop. Stroke. 2023;54(12):3202–13. https://doi.org/10.1161/STROKEAHA.123.044279.

Publisher's Note